Published in final edited form as:
J Histochem Cytochem. 2002 May ; 50(5): 617–628.

Localization of Caveolin 1 in Aortic Valve Endothelial Cells Using Antigen Retrieval

Nalini M. Rajamannan,
Department of Cardiology and Cardiovascular Diseases, Mayo Foundation and Clinic, Rochester, Minnesota

Margaret J. Springett,
Electron Microscopy Core Facility, Mayo Foundation and Clinic, Rochester, Minnesota

Larry G. Pederson, and
Department of Biochemistry and Molecular Biology, Mayo Foundation and Clinic, Rochester, Minnesota

Stephen W. Carmichael
Department of Anatomy, Mayo Foundation and Clinic, Rochester, Minnesota

Summary

Ultrastructural analysis of aortic valve endothelial cells subjected to growth arrest revealed many vesicles defined as caveolae by the localization of caveolin. Translocation of caveolin after exposure to oxidized LDL suggests that the localization of caveolin may be a valuable tool to study models of early atherogenesis. In this study, several antigen retrieval protocols were tested in osmium-fixed and Spurr-embedded cells to determine the optimal method of antigen retrieval in our model system. SDS produced the most consistent labeling pattern. A quantitative evaluation revealed that SDS significantly increased the labeling density in Spurr-embedded cells. The labeling pattern appeared as clusters of gold particles, 15–40 nm in diameter, that were associated with membranes of a similar size which may represent the neck region of the caveolae.

Keywords

antigen retrieval; caveolin 1; immunoelectron microscopy; aortic valve endothelial cells; caveolae; quantitation; plasmalemmal vesicles; gold labeling; ultrastructure; LR White; Spurr resin

Aortic valvular heart disease is the third most common indication for valve replacement in the United States. Whereas the etiology of the degeneration is not well understood, the histology of removed valves shows atherosclerotic lesions and calcification similar to the vascular changes seen in cardiac heart disease. The normal aortic valve is composed of collagen, elastin, and fibroblasts and has layers of endothelial cells on both surfaces between blood and the stroma (Cooper et al. 1966). The aortic valve endothelial cells (AVECs) form a continuous monolayer (Lupu and Simionescu 1985) that acts as a barrier between the blood and the stroma, including subendothelial fibroblasts of the normal heart valve (Manduteanu et al. 1988). Changes in the permeability across valve endothelial cells and vascular endothelial cells are known to be primary events in the formation of experimental atherosclerotic plaque (Vasile et al. 1983; Sarphie 1987). When the integrity of the

Correspondence and present address: Nalini Rajamannan, MD, Northwestern U. Medical School, 675 N St Clair St. Suite 10-240, Chicago, IL 60611. n-rajamannan@northwestern.edu.

endothelial barrier has been compromised in hypercholesterolemic rabbits, foam cells and blood cells accumulate in the subendothelial space (Sarphie 1985). These structural changes are characteristic of the early stages of atherosclerotic plaque formation (Simionescu et al. 1986).

On the luminal surface of normal vascular endothelial cells, the adherence of cationic ferritin indicates a cell surface that is negatively charged, except over the openings of the plasmalemmal vesicles (Simionescu et al. 1981). A similar anionic coat can be demonstrated on endothelial surfaces of normal rabbit aortic valve (Sarphie 1985). In experimental hypercholestrerolemic rabbits, this coat is reduced and results in an increased adhesion of low-density lipoproteins (LDLs) to the endothelial surface of aortic valves (Sarphie 1986). The removal of this surface anionic coat with specific enzymes also resulted in increased LDL attachment to the cell surface (Sarphie 1986). A reduction in anionic surface coat was accompanied by an increased uptake of LDL–gold by the valve endothelial cells. LDL–gold conjugate was demonstrated in vesicles, endosomes, and in subendothelial spaces under the aortic valve endothelium of hypercholesterolemic rabbits, suggesting endocytosis and transcytosis of LDL (Sarphie 1986). The study of vesicle transport across endothelial cells of the aortic valve may be critical to the understanding of atherogenesis.

Atherosclerosis is also linked to a decrease in endothelial nitric oxide (NO) production (Vane et al. 1990; Cayette et al. 1994; Griffith and Stuehr 1995). Endothelial NO synthase (eNOS) is the enzyme that produces NO (Palmer et al. 1987). In normal inactivated endothelial cells, eNOS is complexed to caveolin, a structural protein associated with caveolae (Ju et al. 1997). When activated by complexing with calmodulin, the eNOS is detached from the caveolin and may produce NO (Michel et al. 1997). Subcellular localization of eNOS to the caveolar compartment has been linked to acylation (Schaul et al. 1996) and phosphorylation of eNOS (Michel et al. 1993). In vascular endothelial cells exposed to oxidized LDL (oxLDL), the caveolin and the eNOS both left the caveolar membrane fractions and appeared in the internal membrane fractions (Blair et al. 1999). This translocation of caveolin induced by oxLDL was accompanied by a loss of eNOS activity that was independent of deacylation or phosphorylation of eNOS (Blair et al. 1999). The localization of caveolin may be a valuable tool in studying the translocation of caveolin in early models of atherosclerosis.

Caveolar structure has been studied extensively and caveolae are described as small flask-shaped vesicles limited by a trilaminar membranes that are often continuous with the cell plasmalemma, hence the name plasmalemmal vesicles (Palade 1953; Bruns and Palade 1968). These are uncoated vesicles ranging from 50 to 100 nm in diameter and are prevelant in vascular endothelial cells (Palade 1953; Bruns and Palade 1968). Clusters of caveolae and larger vacuoles form complicated networks that may span the entire width of some endothelial cells. Morphometric analysis of these vesiculo-vacuolar organelles (VVOs) shows that the size of smaller vesicles is similar to that of classical caveolae (Dvorak et al. 1996; Feng et al. 1996). Whereas size and shape have structurally defined caveolae, the localization of caveolin 1 supports the morphological identification (Rothberg et al. 1992). Caveolin 1 is an homooligomer of heavily crosslinked monomers (Sargiacomo et al. 1995) that binds cholesterol (Murata et al. 1995) and binds eNOS in its inactive form (Ju et al. 1997). Without cholesterol, the caveolar structure collapses (Rothberg et al. 1990). Therefore, the structural integrity of the caveolae may be dependent on an interaction between membranous cholesterol and caveolin 1.

Caveolin 1 has been labeled extensively for transmission electron microscopy using frozen sections (Brown et al. 1996; Amino et al. 1997; Scherer et al. 1997; Stang et al. 1997; Luetterforst et al. 1999; Stahlhut and Van Deurs 2000), frozen replicas (Fujimoto and

Fujimoto 1997; Fujimoto et al. 1998; Takayama et al. 1999; Westermann et al. 1999), pre-embedding labeling (Haasemann et al. 1998; Vasile et al. 1999; Dolo et al. 2000; Schwab et al. 2000), postembedding labeling in LR White (Wu et al. 1997; Newmann et al. 1999; Thyberg 2000), postembedding labeling in LR Gold (deWeerd and Leeb–Lundberg 1997), and postembedding labeling in Lowicryls (Golfert et al. 1997; Kasper et al. 1997; Lupu et al. 1997). With these techniques the labeling of caveolin 1 appears to be associated with caveolae, but none of these protocols labeled caveolin 1 in osmium-fixed and Spurr-embedded valve endothelial tissues where ultrastructural details are more apparent.

Ultrastructural details are excellent when tissues are fixed in osmium tetroxide and embedded in epoxy resin, but etching is often necessary to increase the antigenicity. After etching with sodium metaperiodate or hydrogen peroxide, an increase in nonspecific labeling of caveolin 1 was reported in lung tissue (Newmann et al. 1999). In other tissues, antigen retrieval (AR) with heated buffers of various pHs has been used extensively in formalin-fixed tissues embedded in paraffin for light microscopy (Shi et al. 1993). In tissues fixed in osmium for transmission electron microscopy (TEM), saturated sodium metaperiodate was used to etch epoxy sections and label for immunoelectron microscopy (Bendayan and Zollinger 1983). A combination of sodium metaperiodate and heated citrate buffer at pH 6 was also effective in greatly enhancing the labeling of IgG that was only minimally labeled without AR or with sodium metaperiodate only (Stirling and Graff 1995). Whereas AR methods have been successful in other tissues and with other antigens, studies using AR to enhance caveolin 1 labeling are limited. In cryostat sections, the labeling of caveolin 1 was greatly enhanced by digesting with sodium dodecyl sulfate (SDS) before staining for caveolin 1 (Brown et al. 1996). In this report, several AR protocols were evaluated for their effect on caveolin 1 labeling of osmium-fixed and epoxy-embedded AVECs for TEM. In particular, the SDS AR method was quantitatively evaluated and compared to no AR in both Spurr-embedded AVECs and AVECs embedded in LR White.

Materials and Methods

Reagent and Antibody Sources

The reagents for these experiments were obtained from the following commercial sources: PBS plus Tween 20 (PBS-T), sodium citrate, SDS, glycine, tannic acid, goat anti-rabbit IgG conjugated to horseradish peroxidase, and sodium metaperiodate were from Sigma Chemical (St Louis, MO). Rabbit anti-caveolin 1 and human endothelial cell lysate were from Transduction Laboratories (Franklin Lakes, NJ). Spurr resin embedding components, DER-736, ERL-4206, NSA, and DMAE, parlodion, glutaraldehyde, uranyl acetate, osmium tetroxide, nickel grids (300-mesh thin bar), lead citrate, and sodium cacodylate were from Electron Microscopy Sciences (Fort Washington, PA). Goat anti-rabbit conjugated to 10-nm and 5-nm colloidal gold, ECL Western blotting detection reagents, and normal goat serum were from Amersham Life Sciences (Arlington Heights, IL), acetone from JT Baker (Phillipsburg, NJ), amyl acetate from Mallinckrodt (Paris, KY), formaldehyde from Ted Pella (Redding,CA), Dulbecco's PBS without calcium or magnesium from BioWhittaker (Walkersville, MD), gels from BioRad (Hercules, CA), serum-free media, medium 199, and fetal bovine serum from Life Technologies (Rockville, MD).

Fixation and Embedding

Aortic valve endothelial cells (AVECs) were cultured from porcine valves after enzymatic digestion as previously described (Johnson and Fass 1983). Briefly, cells were maintained in medium 199 with 10% fetal bovine serum at 37C in a humidified atmosphere of 5% carbon dioxide in air. In these experiments, the cells were used between passages 3 and 4. To arrest

cell growth, cells were treated with serum-free medium for 24 hr before harvesting for the labeling experiments.

Normal AVECs were incubated for 24 hr in serum-free medium and fixed overnight in 4% formaldehyde plus 1% glutaraldehyde in phosphate buffer (McDowell and Trump 1976). Specimens were rinsed in phosphate buffer, postfixed in 1% osmium tetroxide, rinsed in water, stained en bloc in 2% aqueous uranyl acetate, dehydrated in a series of ethanols to 100%, infiltrated, and embedded in Spurr resin (Spurr 1969).

A duplicate set of serum-free cells was fixed overnight in 4% formaldehyde plus 0.2% glutaraldehyde in phosphate buffer. Cells were rinsed in phosphate buffer and dehydrated in a series of ethanols to 80% while progressively lowering the temperature to −20C. The cells were infiltrated in LR White resin at −20C overnight, embedded in fresh resin at room temperature (RT), and polymerized at 50C for 2 days. This embedding protocol has been used successfully to label collagen Type IV (Hann et al. 2001).

Sections with a silver interference color (∼80 nm thick) were mounted on 300-mesh nickel grids for labeling. Some grids were mounted on parlodion membranes before labeling to minimize section wrinkling. These membranes were made from 1.5% parlodion dissolved in 1:1 acetone:amyl acetate. Both grid and section were deposited on the dried parlodion films on the platform. Gold conjugate (5 nm) was dried onto a membrane and negatively stained with uranyl acetate. The diameter of the cloud around the dense particle was measured.

Antigen Retrieval

For a comparison of AR protocols, grids were exposed to sodium metaperiodate, heated citrate buffer, or a combination of sodium metaperiodate and heated citrate buffer. Sections were treated in a saturated aqueous solution of sodium metaperiodate for 10 minutes (Bendayan and Zollinger 1983) and rinsed in four changes of filtered water. Grids were boiled for 10 min in 0.01 M citrate buffer and cooled for 15 min (Shi et al. 1993). Grids subjected to dual treatments were first treated in sodium metaperiodate, rinsed in water, and then heated in citrate buffer (Stirling and Graff 1995). Grids for quantitative comparison were either incubated for 60 min in 1% SDS in PBS-T (pH 7.4) at RT (Brown et al. 1996) or not subjected to any AR, then rinsed in PBS-T before labeling with colloidal gold.

Immunoelectron Microscopy

The antibody to caveolin 1 was a rabbit polyclonal to the N-terminus of human caveolin 1 that included amino acid sequences 1–97. This antibody was diluted 1:50 in PBS-T. Blocking buffer was PBS with added 0.05% Tween-20 (PBS-T), 1% glycine, and 2% normal goat serum. The secondary antibody was goat anti-rabbit conjugated to 5- or 10-nm colloidal gold and was diluted 1:100 in PBS-T. After AR grids were incubated in blocking buffer for 15 min. The grids were incubated in primary antibody for 3 hr at RT. Grids were rinsed in four changes of PBS-T, incubated for 60 min in secondary goat anti-rabbit conjugated to 5-nm gold, rinsed in PBS-T, rinsed in water, and dried. Some sections were examined after staining with uranyl acetate and lead citrate and some were examined without any post-labeling staining. After AR in a combination of sodium metaperiodate and heated citrate buffer, controls were labeled with a nonspecific rabbit antibody and with the omission of primary antibody. Controls were also incubated in SDS and labeled without primary antibody.

Quantitative Methods

The minor diameter of all vesicle membranes was measured in 39 fields of 1 μm^2 of Spurr-embedded cells subjected to SDS. One group of membranes surrounded dense vesicle matrix

and the other group surrounded clear areas within the vesicle. When gold labeling density (gold particles/μm^2) in the different embedding and antigen retrieval media was compared, the gold particles were counted in 25 fields. Within the gold clusters, the distance between the center of the gold particle to the center of the nearest neighboring gold particle was measured. All statistical comparisons were made with the two-tailed Student's *t*-test assuming unequal variances.

Results

General Structural Appearance and Size

Porcine AVECs under normal culture conditions usually contain many mitochondria, Golgi apparatus, and an occasional group of caveolae (Figure 1A). When these cell cultures were growth-arrested by exposure to serum-free medium for 24 h before fixation, the ultrastructural examination revealed many caveolae (Figures 1C and 1D) and an occasional vesiculo-vacuolar organelle (VVO) (Figure 1B). When sectioned at a right angle to the plasma or vacuolar membrane, single caveolae appeared as flask-shaped invaginations of the membranes (Figure 1D). In this orientation, the neck of the caveola opened either into the exterior of the cell or into a larger vacuole. When sectioned through the midline of the caveolae, the single vesicles were more circular and the vesicle matrix was either homogeneously dense or had a clear area within the dense matrix of the vesicle (Figure 1C). This clear area may represent the caveolar stomata, and in rare cases a dense central knob can be demonstrated within these clear areas (Figure 4B).

When AVECs were processed in LR White for maximal antigenicity (Figure 2), a lack of membrane contrast in mitochondria, caveolae, and plasmalemma was apparent. The labeling pattern for caveolin was clustered and usually found near the plasmalemma (Figure 2), but assessing the specificity of the label was difficult when the trilaminar membrane structure was not well contrasted. LR White resin does not polymerize when osmium is used for postfixation. Without osmium and with partial dehydration, the trilaminar structure of the membranes appeared in reverse contrast with a dark middle layer and pale outer layers (Figure 2 inset, white arrow).

Antigen Retrieval

In Spurr-embedded cells, several AR methods were tested in the search for a protocol that would retain the membrane structure of the vesicles and increase the labeling density for caveolin. AR in sodium metaperiodate showed a good labeling pattern but produced a dense precipitate that was difficult to remove completely from the sections. A nonspecific labeling was often associated with this electron-dense debris. When heated citrate buffer was used as a single AR treatment, the specificity of the label appeared to be improved over sodium metaperiodate used alone. A combination of sodium metaperiodate followed by heated citrate buffer was effective in producing a specific caveolin label, but section wrinkling often obstructed an evaluation of the labeling pattern. The most consistent labeling pattern was found after AR in SDS, and caveolin was consistently localized over vesicle profiles with little contamination and no section wrinkling.

Labeling Pattern

In AVECs subjected to serum-free medium, the labeling of caveolin 1 was most often associated with membranes of caveolae. Signal was not found on every caveola and was not associated with the larger vacuoles or clathrin-coated pits. This pattern was similar in cells embedded in both LR White and Spurr resins, but the labeling density in Spurr resin was significantly decreased compared to the labeling density in LR White-embedded cells. Control cells labeled without primary antibody were negative with SDS AR.

After AR in SDS, caveolin labeling was demonstrated in AVECs that had been embedded in Spurr resin. The labeling was clustered and consistently localized over vesicle membranes. Figure 3 shows some typical labeling patterns found in Spurr-embedded cells. Whereas the label was found dispersed as single gold particles over a vesicle membrane (Figures 3A and 3B), some clusters of gold particles were found over membranes surrounding dense areas of the vesicle (Figures 3C–3E) However, most of the clusters were associated with membranes of smaller diameter that surrounded clear areas in the vesicle (Figures 3A–3F). These gold clusters were not amorphous aggregations of gold but were often aligned linearly (Figure 3F) and separated by distances greater than 15 nm from the next nearest neighboring gold particle. In Figure 4B, a vesicle was sectioned through the dense knob and the radiating filamentous structures appeared similar to those published earlier by Palade and Bruns (1968). Figure 4A shows a double semicircular labeling pattern over small filamentous cross-sections (Figure 4B, arrow). These filamentous structures were smaller than the 5-nm gold particles and may represent some element of the dense knob structure. Although this pattern is rare (Figure 4), it demonstrates the structural information that might be obtained with the caveolin labeling in Spurr-embedded cells.

Quantitative Comparisons

Figure 5 shows the distribution of two membrane populations that were measured in AVECs embedded in Spurr resin and labeled for caveolin after SDS AR. These membranes' profiles are parts of the same vesicles but they may represent two regions of the vesicle that can be separated by size. The diameters of vesicle membranes surrounding a dense matrix may represent the body of the vesicle, and the membranes surrounding a clear area within the vesicle probably represent the narrowing of the membranes in the neck region of the vesicle. Figure 5 suggests that these two vesicle regions on the same vesicles can be separated by size, and the two membrane groups are significantly different, as shown in Table 1. The two groups were compared statistically with the two-tailed Student's *t*-test assuming unequal variances.

Because LR White is considered optimal for preserving antigenicity, the gold labeling density of caveolin was determined with and without SDS antigen retrieval. These densities were compared to gold labeling density in Spurr-embedded cells with and without SDS retrieval. The quantitative results are summarized in Table 2 and graphically represented in Figure 6.

The density of gold particles/μm^2 was significantly different when the two embedding media were compared ($p<0.001$), but the AR in SDS did not significantly increase the labeling efficiency in the LR White-embedded cells ($p=0.763$). In Spurr-embedded cells, a significant increase in labeling density could be demonstrated ($p<0.001$) when SDS was used as an AR medium. Given the nature of the structural data present in Spurr-embedded cells, an increase in labeling density after SDS treatment may be a valuable tool in our study of AVECs.

In Spurr-embedded cells with AR in SDS, many single gold particles were found over caveolae membranes and were isolated from their nearest neighboring gold particle by distances of over 100 nm. Gold particles that were closer than 100 nm were designated as gold clusters, and 61 clusters were identified that included 71% of the gold particles counted. Within the gold clusters, the distances between the particles and their nearest neighbor was measured and a distribution of those distances appears in Figure 7. The clusters are concentrated between 5 and 30 nm.

The cloud around the gold probe (5 nm) was negatively stained and the diameter of the "cloud" was measured in 172 particles. Table 3 summarizes the size of the negatively stained cloud around the 5-nm gold particle.

If this cloud represents the distance at which gold can be aggregated, then gold particles closer than 15 nm will be, for this discussion, considered aggregated. Particles with interpoint distances greater than 15 nm will be considered as labeling associated with a clustered epitope on the section surface. Clustered labeling of caveolin is quite apparent at 15–40 nm but is almost nonexistent at distances of 40–80 nm. These data are not conclusive but support the theory that caveolin labeling is associated with the smaller membranes surrounding the clear areas within the vesicle (20–40 nm) and suggest that these areas may represent the narrower neck of the caveolae.

Discussion

After arresting cell growth with serum-free medium, a considerable number of caveolae present as single caveola, groups of caveolae, or VVOs were demonstrated in AVECs. In these cells, caveolin label is associated with membrane-limited clear zones that are smaller and often enclosed within the larger vesicle membrane that defines the vesicle matrix. The diameters of these smaller membranes (20–40 nm) are similar to those stomata or vesicle openings (30–50 nm) observed in freeze-fractured preparations (Severs and Simons 1986). Vascular smooth muscle cells preferentially fracture through the stomata and are surrounded by small circles of intramembranous particles 30-50 nm in diameter (Severs and Simons 1986). These rings of intramembranous particles have been labeled for caveolin 1 (Fujimoto and Fujimoto 1997; Fujimoto et al. 1998; Westermann et al. 1999). A ring-like pattern is also suggested by the oligomeric structure of caveolin. Caveolin 1 is a small monomer of 21–24 kD, but, when isolated from cells, it is a much larger homo-oligomer of 300–325 kD (Sargiacomo et al. 1995). These monomers may be crosslinked by both the N- and C-termini of caveolin 1 (Song et al. 1997) and will self-assemble into larger oligomers. When examined by electron microscopy, the larger oligomers are nonlinear polymers 25 nm in diameter (Sargiacomo et al. 1995). Our data supports the presence of caveolin as a clustered epitope that is 15–40 nm in diameter and is associated with membranes 20–40 nm in diameter that limit a clear zone within the vesicle.

Caveolin has been associated with the cytoplasmic side of the caveolar membrane, and ultrastructural studies of caveolae revealed four to six filaments arranged concentrically on the cytoplasmic surface. When this striated coat was disrupted, the labeling of caveolin was greatly increased (Rothberg et al. 1992). The nature of this striated coat has not been fully analyzed but recent studies have shown that caveolin is co-localized with filamin, a protein associated with F-actin crosslinking (Stahlhut and Van Deurs 2000). In our preparations the caveolae are often aligned along cellular filaments and, rarely, caveolin label is associated with filamentous rods smaller in diameter than the 5-nm gold particles. Similar structures were reported to be part of the caveolar striated coat (Rothberg et al. 1992). Palade and Bruns (1968) also showed some small filaments radiating from the stomata area and reported that these might be elements of the dense knob structures of the diaphragm that guard the opening of the vesicle. In Figure 4, these structures appear to be part of the dense knob structure. In LR White-embedded cells, these microfilaments were not definable. The preservation of ultrastructural detail combined with the labeling of caveolin is critical to defining a relationship between caveolin and other cell components.

Our data suggest that the postembedding labeling of caveolin may be dependent on the orientation of the caveolae within the section. When the neck regions of the caveolae are exposed at the section surface, the epitope has access to the labeling solutions and the

caveolin is labeled. The exposure of the epitope at the section surface may not be the only factor that governs the positive labeling of caveolin. Perhaps attachments between the monomers or other ligands attached to caveolin complex must be dissociated before the antibody has access to the N-terminus of the caveolin molecule. SDS is commonly used to dissociate proteins, but the caveolin complex of 14 or 15 monomers is somewhat resistant to dissociation by SDS (Sargiacomo et al. 1995). Caveolin forms complexes with cholesterol, the cell cytoskeleton, and molecules involved in the cell signaling process. In our AVECs embedded in LR White, caveolin labeling was not increased after AR with SDS. These data suggest that SDS has no effect on disassociation of the caveolin complex or other ligands but instead may have an effect on the osmium fixation or epoxy embedding. Because SDS is known to increase the labeling of caveolin in aldehyde-fixed cryosections (Brown et al. 1996), perhaps fixation is inhibitory to caveolin labeling and SDS is effective in severing bonds between the fixative and caveolin.

Several AR techniques other than SDS were also effective in localizing caveolin 1 in AVECs fixed in osmium tetroxide and embedded in Spurr resin. AR with heated citrate buffer alone and with a combination of sodium metaperiodate followed by heated citrate buffer were equally effective in increasing the labeling of caveolin 1. When many AR methods were compared on tissue embedded in Araldite, the best quantitative increases in label were produced by a combination of sodium metaperiodate and heated citrate buffer (Stirling and Graff 1995). The exact mechanism of AR with heated citrate buffer is speculative but some have theorized that AR disrupts the bonds between proteins that are produced by aldehyde fixation. Another theory suggests that bonds between tissue proteins and the epoxy embedding resin are responsible for diminished antigenicity. In ethanol-fixed tissues, in which bonds between proteins are weaker than those produced by aldehyde fixation, AR in heated citrate buffer also produced an increased amount of label (Brorson 1999).

In Spurr-embedded AVECs, sodium metaperiodate used alone showed an increase in caveolin 1 labeling. However, an electron-dense contamination often obscured the structural detail and this precipitate was labeled nonspecifically by gold particles. This electron-dense precipitate may be osmium that was removed from the section by sodium metaperiodate. Others have reported that sodium metaperiodate is effective in removing the effects of osmium fixation (Bendayan and Zollinger 1983). After a combination of sodium metaperiodate and boiling in citrate buffer, the electron-dense precipitate is removed from the section surface. However, sections exposed to the hot citrate buffer were wrinkled. Attaching the section to a supporting film of parlodion before AR minimized the section wrinkling. In our work, the best localization of caveolin 1 was achieved after AR in SDS. Contamination was minimal, sections were not wrinkled, and no supporting film was necessary.

Acknowledgments

We wish to thank Dr Ann Dvorak for her helpful comments on the manuscript, and Jon Charlesworth of Mayo Foundation's Electron Microscopy Core Facility.

Literature Cited

Amino K, Honda Y, Ide C, Fujimoto T. Distribution of plasmalemmal Ca(2+)-pump and caveolin in the corneal epithelium during the wound healing process. Curr Eye Res. 1997; 16:1088–1095. [PubMed: 9395767]

Bendayan M, Zollinger M. Ultrastructural localization of antigenic sites on osmium-fixed tissues applying the protein A-gold technique. J Histochem Cytochem. 1983; 31:101–109. [PubMed: 6187796]

Blair A, Shaul PW, Yahanna IS, Conrad PA, Smart EJ. Oxidized low density lipoprotein displaces endothelial nitric-oxide synthase (eNOS) from plasmalemmal caveolae and impairs eNOS activation. J Biol Chem. 1999; 274:32512–32519. [PubMed: 10542298]

Brorson SH. Fixative-dependent increase in immunogold labeling following antigen retrieval on acrylic and epoxy sections. Biotech Histochem. 1999; 74:248–260. [PubMed: 10711505]

Brown D, Lydon J, McLaughlin M, Stuart–Tilley A, Tyszkowski R, Alper S. Antigen retrieval in cryostat sections and cultured cells by treatment with sodium dodecyl sulfate (SDS). Histochem Cell Biol. 1996; 105:261–267. [PubMed: 9072183]

Bruns RR, Palade GE. Studies on blood capillaries: I General organization of blood capillaries in muscle. J Cell Biol. 1968; 37:244–276. [PubMed: 5656394]

Cayette AJ, Palacino JJ, Horten K, Cohen RA. Chronic inhibition of nitric oxide production accelerates neointima formation and impairs endothelial function in hypercholesterolemic rabbits. Arterioscler Thromb. 1994; 14:753–759. [PubMed: 7513551]

Cooper T, Napolitano LM, Fitzgerald MJ, Moore KE, Daggett WM, Willman VL, Sonnenblick EH, Hanlon CR. Structural basis of cardiac valve function. Arch Surg. 1966; 93:767–771. [PubMed: 5331873]

deWeerd WF, Leeb-Lundberg LM. Bradykinin sequesters B2 brandykinin receptors and the receptor-coupled Galpha subunits Galphaq and Galphai in caveolae in DDT1 MF-2 smooth muscle cells. J Biol Chem. 1997; 272:17858–17866. [PubMed: 9211942]

Dolo V, Li R, Dillinger M, Flati S, Manela J, Taylor BJ, Pavan A, Ladisch S. Enrichment and localization of ganglioside G(D3) and caveolin-1 in shed tumor cell membrane vesicles. Biochim Biophys Acta. 2000; 1486:265–274. [PubMed: 10903477]

Dvorak AM, Kohn S, Morgan ES, Fox P, Nagy JA, Dvorak HF. The vesiculo-vacuolar organelle (VVO): a distinct endothelial cell structure that provides a transcellular pathway for macromolecular extravasation. J Leukocyte Biol. 1996; 59:100–115. [PubMed: 8558058]

Feng D, Nagy J, Hipp J, Dvorak H, Dvorak A. Vesiculo-vacuolar organelles and the regulation of venule permeability to macromolecules by vascular permeability factor. Histamine and serotonin. J Exp Med. 1996; 183:1981–1986. [PubMed: 8642308]

Fujimoto T, Fujimoto K. Metal sandwich method to quick-freeze monolayer cultured cells for freeze fracture. J Histochem Cytochem. 1997; 45:595–598. [PubMed: 9111237]

Fujimoto T, Hagiwara H, Aoki T, Kogo H, Nomura R. Caveolae: from a morphological point of view. J Electron Microsc. 1998; 5:451–460.

Golfert F, Kasper M, vanEys GJ, Funk RH. Cytoskeletal characterization of arteriovenous epitheloid cells. Histochem Cell Biol. 1997; 108:513–523. [PubMed: 9450634]

Griffith OW, Stuehr DJ. Nitric oxide synthases: properties and catalytic mechanisms. Annu Rev Physiol. 1995; 57:707–736. [PubMed: 7539994]

Haasemann M, Cartaud J, Muller–Esterl W, Dunia I. Agonist-induced redistribution of bradykinin B2 receptor in caveolae. J Cell Sci. 1998; 111:917–928. [PubMed: 9490636]

Hann CR, Springett MJ, Johnson DH. Antigen retrieval of basement membrane proteins from archival eye tissues. J Histochem Cytochem. 2001; 49:475–482. [PubMed: 11259450]

Johnson CM, Fass DN. Porcine cardiac valvular endothelial cells in culture. A relative deficiency of fibronectin synthesis in vitro. Lab Invest. 1983; 49:589–598. [PubMed: 6314039]

Ju H, Zou R, Venema RJ, Venema RC. Direct interaction of endothelial nitric-oxide synthase and caveolin-1 inhibits synthase activity. J Biol Chem. 1997; 272:18522–18525. [PubMed: 9228013]

Kasper M, Golfert F, Funk RH. Immunoelectron microscopical characterization of the epithelioid type of smooth muscle cells in human glomus organs. Ultrastruct Pathol. 1997; 21:425–430. [PubMed: 9273972]

Luetterforst R, Stang E, Zorzi N, Carozzi A, Way M, Parton RG. Molecular characterization of caveolin association with the Golgi complex: identification of a cis-Golgi targeting domain in the caveolin molecule. J Cell Biol. 1999; 145:1443–1459. [PubMed: 10385524]

Lupu C, Goodwin CA, Westmuckett AD, Emeis JJ, Scully MF, Kakkar VV, Lupu F. Tissue factor pathway inhibitor in endothelial cells colocalizes with glycolipid microdomains/caveolae. Regulatory mechanism(s) of the anticoagulant properties of the endothelium. Arterioscler Thromb Vasc Biol. 1997; 17:2964–2974. [PubMed: 9409283]

Lupu F, Simionescu M. Organization of the intercellular junctions in the endothelium of cardiac valves. J Submicrosc Cytol. 1985; 17:119–132. [PubMed: 3999177]

Manduteanu I, Popov D, Radu A, Simionescu M. Calf cardiac valvular endothelial cells in culture: production of glycosaminoglycans, prostacyclin and fibronectin. J Mol Cell Cardiol. 1988; 20:103–118. [PubMed: 2840511]

McDowell EM, Trump BF. Histologic fixatives suitable for diagnostic light and electron microscopy. Arch Pathol Lab Med. 1976; 100:405–414. [PubMed: 60092]

Michel J, Feron O, Sase K, Prabhakar P, Michel T. Caveolin versus calmodulin: counterbalancing allosteric modulators of nitric oxide synthase. J Biol Chem. 1997; 272:25907–25912. [PubMed: 9325323]

Michel T, Li GK, Busconi L. Phosphorylation and subcellular translocation of endothelial nitric-oxide synthase. Proc Natl Acad Sci USA. 1993; 90:6252–6256. [PubMed: 7687064]

Murata M, Peranen J, Schreiner R, Weiland F, Kurzchalia TV, Simons K. VIP21/Caveolin 1 is a cholesterol-binding protein. Proc Natl Acad Sci USA. 1995; 92:10339–10343. [PubMed: 7479780]

Newmann GR, Campbell L, von Ruhland C, Jasani B, Gumbleton M. Caveolin 1 and its cellular and subcellular immunolocalization in lung alveolar epithelium: implications for alveolar epithelial type I cell function. Cell Tissue Res. 1999; 295:111–120. [PubMed: 9931357]

Palade GE. Fine structure of blood capillaries. J Appl Phys. 1953; 24:1424.

Palade GE, Bruns RR. Structural modulations of plasmalemma vesicles. J Cell Biol. 1968; 37:633–649. [PubMed: 11905197]

Palmer RMJ, Ferrige AG, Mondada S. Nitric oxide release accounts for the biological activity of endothelium-derived relaxing factor. Nature. 1987; 327:524–526. [PubMed: 3495737]

Rothberg KG, Heuser JE, Donzell WC, Ying YS, Glenney JR, Anderson RG. Caveolin, a protein component of caveloae membrane coats. Cell. 1992; 68:673–682. [PubMed: 1739974]

Rothberg KG, Ying YS, Kamen BA, Anderson GW. Cholesterol controls the clustering of the glycophospholipid-anchored membrane receptor for 5-methyltetrahydrofolate. J Cell Biol. 1990; 111:2931–2938. [PubMed: 2148564]

Sargiacomo M, Scherer PE, Tang ZL, Kubler E, Song KS, Sanders MC, Lisanti MP. Oligomeric structure of caveolin 1: implications for caveolae membrane organization. Proc Natl Acad Sci USA. 1995; 92:9407–9411. [PubMed: 7568142]

Sarphie TG. Anionic surface properties of aortic and mitral valve endothelium from New Zealand White rabbits. Am J Anat. 1985; 174:145–160. [PubMed: 3840642]

Sarphie TG. A cytochemical study of the surface properties of aortic and mitral valve endothelium from hypercholesterolemic rabbits. Exp Mol Pathol. 1986; 44:281–296. [PubMed: 3720917]

Sarphie TG. Interactions of IgG and B-VLDL with aortic valve endothelium from hypercholesterolemic rabbits. Atherosclerosis. 1987; 68:199–212. [PubMed: 3322301]

Schaul PW, Smart EJ, Robinson LJ, German Z, Yuhanna I, Ying Y, Anderson RGW, Michel T. Acylation targets endothelial nitric-oxide synthase to plasmalemmal caveolae. J Biol Chem. 1996; 271:6518–6522. [PubMed: 8626455]

Scherer PE, Lewis RY, Volonte D, Engelman JA, Galbiati F, Couet J, Kohtz DS, vanDonselaar E, Peters P, Lisanti MP. Cell-type and tissue-specific expression of caveolin-2. Caveolins 1 and 2 co-localize and form a stable hetero-oligomeric complex in vivo. J Biol Chem. 1997; 272:29337–29346. [PubMed: 9361015]

Schwab W, Kasper M, Gavlik JM, Schulze E, Funk RH, Shakbaei M. Characterization of caveolins from human knee joint cartilage: expression of caveolin-1, -2 and -3 in chondrocytes and association with integrin beta 1. Histochem Cell Biol. 2000; 113:221–225. [PubMed: 10817676]

Severs NJ, Simons HL. Caveolar bands and the effects of sterol-binding agents in vascular smooth muscle plasma membrane. Lab Invest. 1986; 55:295–307. [PubMed: 3747448]

Shi SR, Chaiwun B, Young L, Cote RJ, Taylor CR. Antigen retrieval technique utilizing citrate buffer or urea solution for immunohistochemical demonstration of androgen receptor in formalin-fixed paraffin sections. J Histochem Cytochem. 1993; 41:1599–1604. [PubMed: 7691930]

Simionescu N, Simionescu M, Palade GE. Differentiated microdomains on the luminal surface of the capillary endothelium: I Preferential distribution of anionic sites. J Cell Biol. 1981; 90:605–613. [PubMed: 7287817]

Simionescu N, Vasile E, Lupu F, Popescu G, Simionescu M. Prelesional events in atherogenesis: accumulation of extracellular cholesterol-rich liposomes in the intima and cardiac valves of hyperlipidemic rabbits. Am J Pathol. 1986; 123:109–125. [PubMed: 3963146]

Song KS, Tang ZL, Li S, Lisanti MP. Mutational analysis of the properties of caveolin 1. J Biol Chem. 1997; 272:4398–4403. [PubMed: 9020162]

Spurr AR. A low-viscosity epoxy resin embedding medium for electron microscopy. J Ultrastruct Res. 1969; 26:31–43. [PubMed: 4887011]

Stahlhut M, Van Deurs B. Identification of filamin as a novel ligand for caveolin-1: evidence for the organization of caveolin-1 associated membrane domains by the actin cytoskeleton. Mol Biol Cell. 2000; 11:325–337. [PubMed: 10637311]

Stang E, Kartenbeck J, Parton RG. Major histocompatibility complex class I molecules mediate association of SV40 with caveolae. Mol Biol Cell. 1997; 8:47–57. [PubMed: 9017594]

Stirling JW, Graff PS. Antigen unmasking for immunoelectron microsocpy: labeling is improved by treating with sodium ethoxide or sodium metaperiodate, then heating on retrieval medium. J Histochem Cytochem. 1995; 43:115–123. [PubMed: 7529784]

Takayama I, Terada N, Baba T, Ueda H, Kato Y, Fujii Y, Ohno S. “In vivo cryotechnique” in combination with replica immunoelectron microscopy for caveolin in smooth muscle cells. Histochem Cell Biol. 1999; 112:443–445. [PubMed: 10651094]

Thyberg J. Differences in caveolae dynamics in vascular smooth muscle cells of different phenotypes. Lab Invest. 2000; 80:915–929. [PubMed: 10879742]

Vane JR, Anggard EE, Botting RM. Regulatory functions of the vascular endothelium. N Engl J Med. 1990; 323:27–36. [PubMed: 2113184]

Vasile E, Qu-Hong, Dvorak HF, Dvorak AM. Caveolae and vesiculo-vacuolar organelles in bovine capillary endothelial cells cultured with VPF/VEGF on floating Matrigel-collagen gels. J Histochem Cytochem. 1999; 47:159–168. [PubMed: 9889252]

Vasile E, Simionescu M, Simionescu N. Visualization of the binding, endocytosis, and transcytosis of low-density lipoprotein in the arterial endothelium in situ. J Cell Biol. 1983; 96:1677–1689. [PubMed: 6853599]

Westermann M, Leutbecher H, Meyer HW. Membrane structure of caveolae and isolated caveolin 1-rich vesicles. Histochem Cell Biol. 1999; 111:71–81. [PubMed: 9930886]

Wu M, Fan J, Gunning W, Ratnam M. Clustering of GPI-anchored folate receptor independent of both cross-linking and association with caveolin. J Membr Biol. 1997; 159:137–147. [PubMed: 9307440]

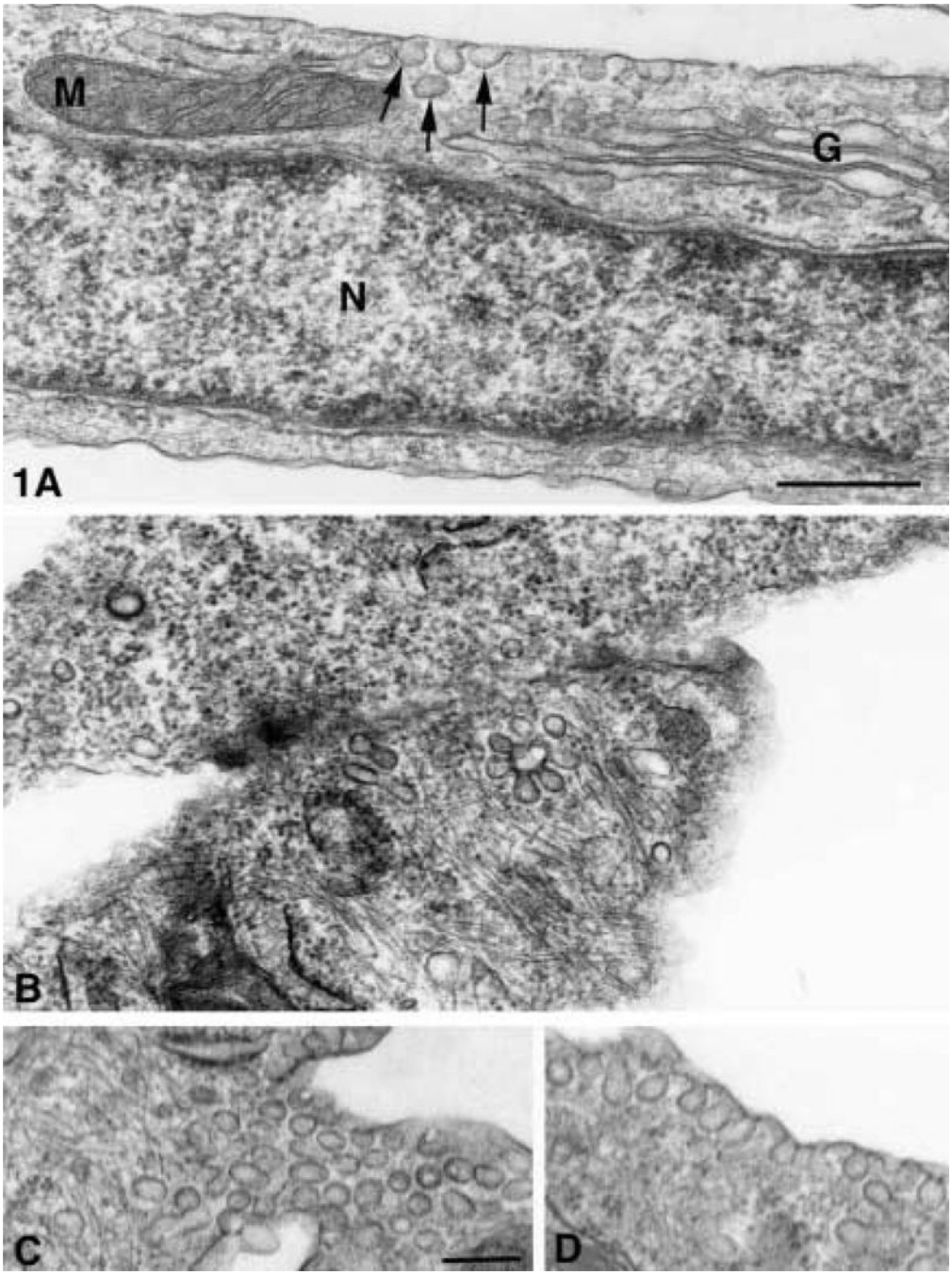

Figure 1.

(**A**) Normal cultured AVECs from pig with ultrastructural detail that can be demonstrated in sections osmium-fixed, uranyl en bloc-stained, and embedded in Spurr resin. Membranes of mitochondria (M), Golgi (G), caveolae (arrows), and those surrounding nucleus (N) show trilaminar structure of lipid bilayers. Bar = 400 nm. (**B**–**D**) Serum-free aortic valve endothelial cell with VVO (arrow) in the border between two endothelial cells (**B**) and caveolae groups (arrow) aligned parallel to (**C**) and caveolae oriented perpendicular to the plasma membrane (**D**). Bar = 100 nm.

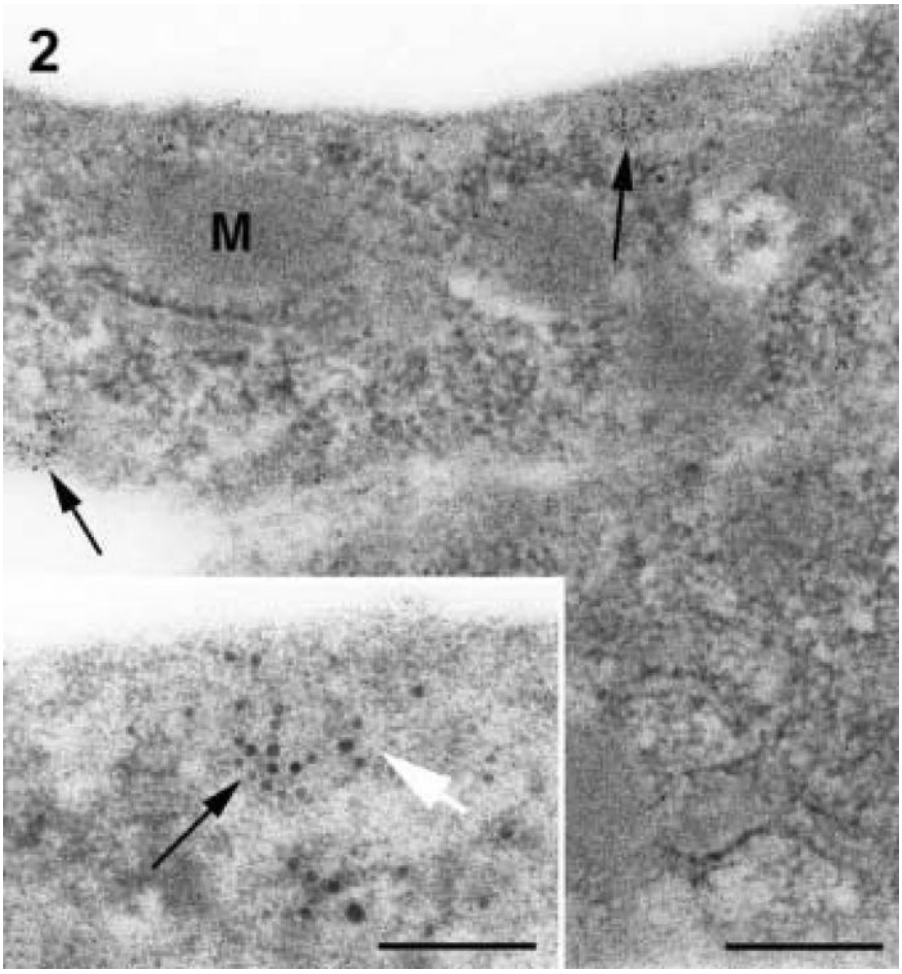

Figure 2.
Serum-free AVEC without osmium and embedded in LR White resin. Membranes of mitochondria (M), caveolae, and plasmalemma have little contrast and are difficult to resolve. The labeling of caveolin (arrows) is patchy and appears to be concentrated in zones near the plasma membranes. Bar = 100 nm. (Inset) Higher magnification of gold labeling (black arrow) in LR White-embedded cells that have no postfixation in osmium showing membranes of reverse contrast (white arrow). Bar = 33 nm.

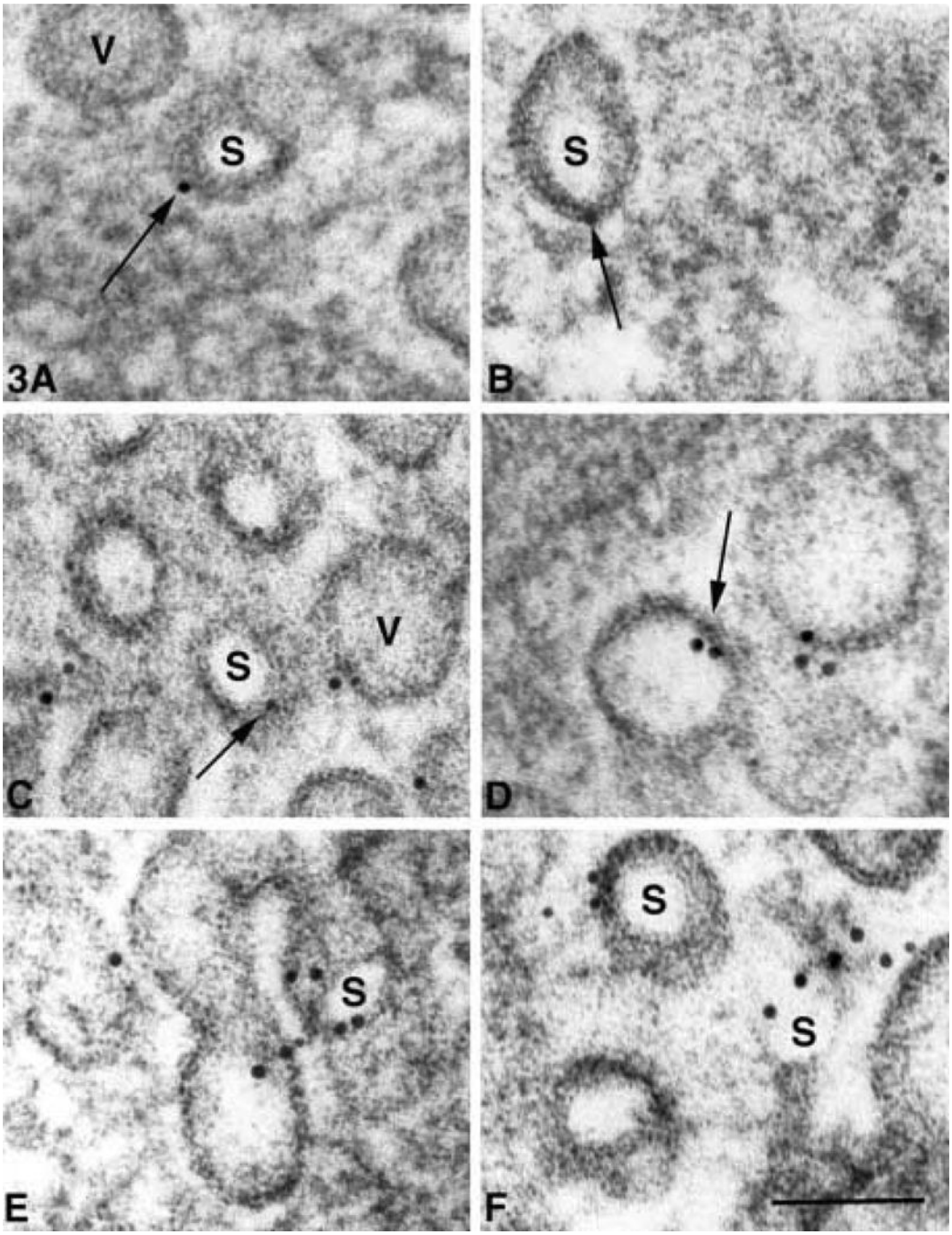

Figure 3.

(**A**–**F**) Caveolin labeling patterns in AVECs under serum-free conditions, embedded in Spurr resin and subjected to pre-labeling AR in SDS. The gold label (arrows) is consistently associated with vesicle membranes that surround the dense vesicle matrix (V) and clear areas (S) that often do not show a central dense knob. These smaller vesicle membranes may represent the neck region of the vesicle when the diaphragm has been removed in sectioning. Bar = 60 nm.

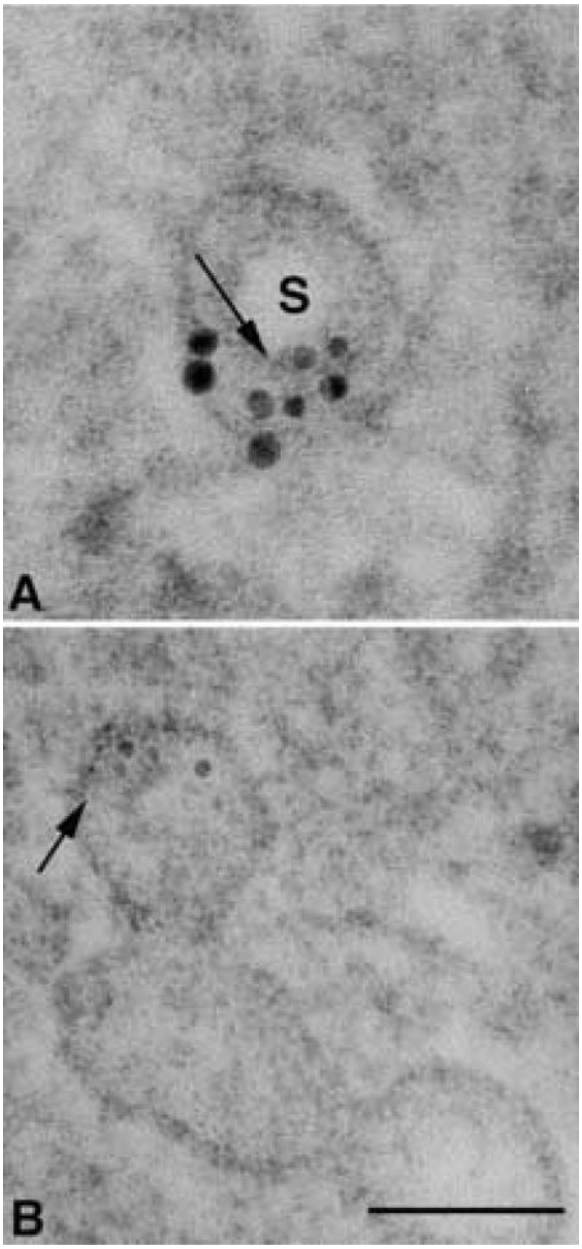

Figure 4.

High magnification of two vesicles that appear to be sectioned through the stoma area. (**A**) In this section, the dense knob is not apparent and the stoma (S) is a clear area. Two semicircular gold clusters may represent the two angles of membrane curvature that mark the entrance into the vesicle through the neck region. (**B**) Labeling over small radiating tubular structures (arrow) with a diameter smaller than the 5-nm gold particles that may be associated with a dense central knob of the diaphragm. Arrow in **A** points to a cross-section of a tubular structure that corresponds with the diameter of the longitudinally oriented tubules demonstrated in **B**. Bar = 75 nm.

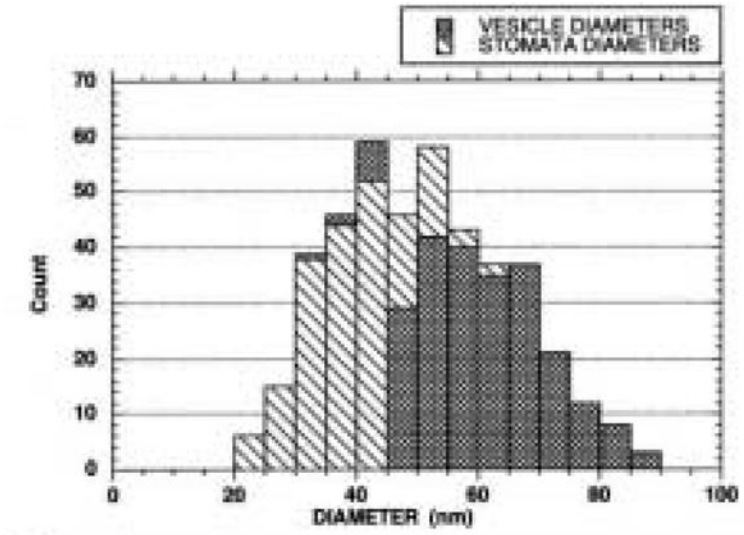

Figure 5.
Distribution of vesicle diameters that define either dense vesicle matrix or clear area within caveolae. Most stomata diameters range from 20 to 40 nm in diameter, while those of the denser vesicle matrix range from 40 to 70 nm in diameter.

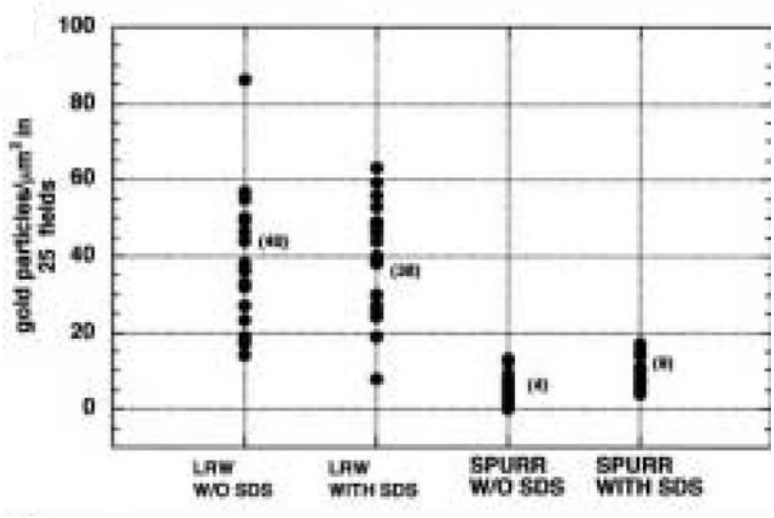

Figure 6.
In LR White- and Spurr-embedded AVECs under serum-free conditions, a comparison of gold-labeling with and without antigen retrieval in SDS. LR White labeling is increased compared to Spurr labeling but there are no differences with and without SDS antigen retrieval. Labeling intensity after Spurr embedding is considerably less than labeling in LR White, but the signal increases after SDS antigen retrieval. The (mean) labeling density in each group is included.

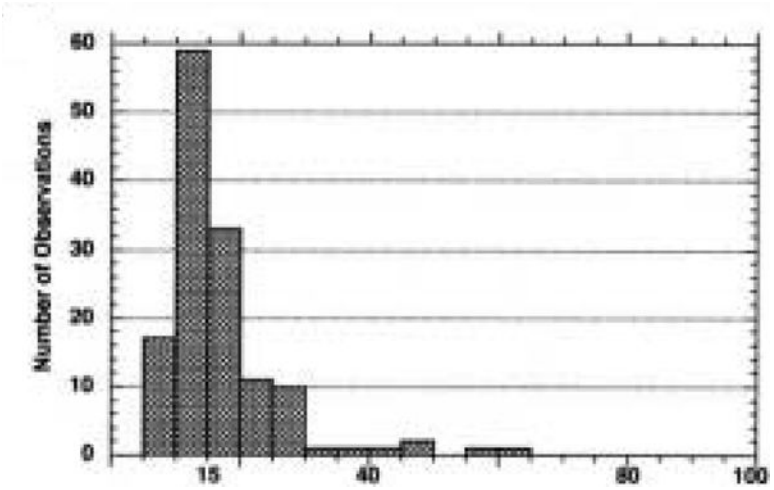

Figure 7.

Distribution of interpoint distances measured between a gold particle and the nearest neighboring gold particle within a gold cluster. Aggregation of 5-nm gold particles due to antibody and gold interactions may occur at distances up to 15 nm, but clusters of particles between 15 and 40 nm may suggest that the clusters are localizing in the neck areas of the vesicles where the membranes are smaller in diameter.

Table 1

A comparison of vesicle diameters

Membrane group	*n*	Mean (μm)	SEM	*p* (*t*-test)
Vesicle	237	60.5	0.67	<0.001
Stomata	193	39.2	0.56	—

Table 2

A comparison of gold labeling density in different embedding procedures with and without antigen retrieval in SDS

Experimental group	*n*	Mean (particles/μm^2)	SEM	Variance	*p* (*t*-test)
LRW without SDS	24	40	4	585	
LRW with SDS	23	38	3	219	0.763
Spurr without SDS	25	4	0	11	
Spurr with SDS	25	9	0	12	<0.001

Table 3
Measurements of cloud diameters surrounding the gold particle

	n	Mean diameter (nm)	SEM	Variance
5-nm gold probe	172	10.32	0.1	1.93